High-speed polarization sensitive optical frequency domain imaging with frequency multiplexing

W.Y. Oh, S.H. Yun, B.J. Vakoc, M. Shishkov, A.E. Desjardins, B.H. Park, J.F. de Boer, G.J. Tearney, and B.E. Bouma

Harvard Medical School and Wellman Center for Photomedicine
Massachusetts General Hospital
50 Blossom Street, BAR 704, Boston, Massachusetts 02114
woh1@partners.org

Abstract: Polarization sensitive optical coherence tomography (PS-OCT) provides a cross-sectional image of birefringence in biological samples that is complementary in many applications to the standard reflectance-based image. Recent *ex vivo* studies have demonstrated that birefringence mapping enables the characterization of collagen and smooth muscle concentration and distribution in vascular tissues. Instruments capable of applying these measurements percutaneously *in vivo* may provide new insights into coronary atherosclerosis and acute myocardial infarction. We have developed a polarization sensitive optical frequency domain imaging (PS-OFDI) system that enables high-speed intravascular birefringence imaging through a fiber-optic catheter. The novel design of this system utilizes frequency multiplexing to simultaneously measure reflectance of two incident polarization states, overcoming concerns regarding temporal variations of the catheter fiber birefringence and spatial variations in the birefringence of the sample. We demonstrate circular cross-sectional birefringence imaging of a human coronary artery *ex vivo* through a flexible fiber-optic catheter with an A-line rate of 62 kHz and a ranging depth of 6.2 mm.

OCIS codes: (170.4500) Optical coherence tomography; (170.3880) Medical and biological imaging; (170.3890) Medical optics instrumentation; (180.3170) Interference microscopy

References and links

1. M.R. Hee, D. Huang, E.A. Swanson, and J.G. Fujimoto, "Polarization-sensitive low-coherence reflectometer for birefringence characterization and ranging," J. Opt. Soc. Am. B **9**, 903-908 (1992).
2. J.F. de Boer, T. E. Milner, M.J.C. van Gemert, and J.S. Nelson, "Two-dimensional birefringence imaging in biological tissue by polarization-sensitive optical coherence tomography," Opt. Lett. **22**, 934-936 (1997).
3. M.J. Everett, K. Schoenenberger, B.W. Colston, Jr., and L.B. Da Silva, "Birefringence characterization of biological tissue by use of optical coherence tomography," Opt. Lett. **23**, 228-230 (1998).
4. C.E. Saxer, J.F. de Boer, B.H. Park, Y.H. Zhao, Z.P. Chen, and J.S. Nelson, "High-speed fiber-based polarization-sensitive optical coherence tomography of *in vivo* human skin," Opt. Lett. **25**, 1355-1357 (2000).
5. B.H. Park, C. Saxer, S.M. Srinivas, J.S. Nelson, and J.F. de Boer, "*In vivo* burn depth determination by high-speed fiber-based polarization sensitive optical coherence tomography," J. Biomed. Opt. **6**, 474-479 (2001).
6. M.C. Pierce, R.L. Sheridan, B.H. Park, B. Cense, and J.F. de Boer, "Collagen denaturation can be quantified in burned human skin using polarization-sensitive optical coherence tomography," Burns **30**, 511-517, (2004).
7. B. Cense, T.C. Chen, B.H. Park, M.C. Pierce, and J.F. de Boer, "*In vivo* depth-resolved birefringence measurements of the human retinal nerve fiber layer by polarization-sensitive optical coherence tomography," Opt. Lett. **27**, 1610-1612 (2002).

#86630 - $15.00 USD Received 20 Aug 2007; revised 7 Nov 2007; accepted 21 Nov 2007; published 14 Jan 2008

8. T.C. Chen, B. Cense, M.C. Pierce, N. Nassif, B.H. Park, S.H. Yun, B.R. White, B.E. Bouma, G.J. Tearney, J.F. de Boer, "Spectral domain optical coherence tomography: ultra-high speed, ultra-high resolution ophthalmic imaging," Archives of Ophthalmology," **123**, 1715-1720 (2005).
9. B. Cense, T.C. Chen, B.H. Park, M.C. Pierce, and J.F. de Boer, "Thickness and birefringence of healthy retinal nerve fiber layer tissue measured with polarization-sensitive optical coherence tomography," Invest. Ophthalmol. Vis. Sci. **45**, 2606-2612 (2004).
10. J. Strasswimmer, M.C. Pierce, B.H. Park, V. Neel, and J.F. de Boer, "Polarization-sensitive optical coherence tomography of invasive basal cell carcinoma," J. Biomed. Opt. **9,** 292-298 (2004).
11. D. Fried, J. Xie, S. Shafi, J.D.B. Featherstone, T.M. Breunig, and C. Le, "Imaging caries lesions and lesion progression with polarization sensitive optical coherence tomography," J. Biomed. Opt. **7**, 618-627 (2002).
12. S. Nadkarni, M.C. Pierce, B.H. Park, J.F. de Boer, E.F. Halpern, S.L. Houser, B.E. Bouma, G.J. Tearney, "Measurement of collagen and smooth muscle cell content in atherosclerotic plaques using polarization-sensitive optical coherence tomography," J. Am. Coll. Cardiol. **49**, 1474-1481 (2007).
13. M.C. Pierce, B.H. Park, B. Cense, and J.F. de Boer, "Simultaneous intensity, birefringence, and flow measurements with high-speed fiber-based optical coherence tomography," Opt. Lett. **27**, 1534-1536 (2002).
14. B.H. Park, M.C. Pierce, B. Cense, J.F. de Boer, "Real-time multi-functional optical coherence tomography," Opt. Express **11**, 782-793 (2003).
15. B.H. Park, M.C. Pierce, B. Cense, and J.F. de Boer, "Jones matrix analysis for a polarization-sensitive optical coherence tomography system using fiber-optic components," Opt. Lett. **29**, 2512-2514 (2004).
16. M.C. Pierce, M. Shishkov, B.H. Park, N.A. Nassif, B.E. Bouma, G.J. Tearney, and J.F. de Boer, "Effects of sample arm motion in endoscopic polarization-sensitive optical coherence tomography," Opt. Express 13, 5739-5749 (2005).
17. B.H. Park, M.C. Pierce, B. Cense, S.H. Yun, M. Mujat, G.J. Tearney, B.E. Bouma, and J.F. de Boer, "Real-time fiber-based multi-functional spectral-domain optical coherence tomography at 1.3 μm," Opt. Express **13**, 3931-3944 (2005).
18. S.H. Yun, G.J. Tearney, J.F. de Boer, N. Iftimia, and B.E. Bouma, "High-speed optical frequency-domain imaging," Opt. Express **11**, 2953-2963 (2003).
19. S.A. Kingsley and D.E.N. Davies, "OFDR diagnostics or fibre and integrated-optic systems," Electron. Lett. 21, 434-435 (1985).
20. S.H. Yun, G.J. Tearney, B.J. Vakoc, M. Shishkov, W.Y. Oh, A.E. Desjardins, M J. Suter, R.C. Chan, J.A. Evans, I.K. Jang, N.S. Nishioka, J.F. de Boer, and B.E. Bouma, "Comprehensive volumetric optical microscopy in-vivo," Nat. Med. **12**, 1429-1433 (2006).
21. J. Zhang, W. Jung, J.S. Nelson, and Z. Chen, "Full range polarization-sensitive Fourier domain optical coherence tomography," Opt. Express **12**, 6033-6039 (2004).
22. S.H. Yun, G.J. Tearney, J.F. de Boer, and B.E. Bouma, "Removing the depth-degeneracy in optical frequency domain imaging with frequency shifting," Opt. Express **12**, 4822-4828 (2004).
23. S.H. Yun, C. Boudoux, G.J. Tearney, and B.E. Bouma, "High-speed wavelength-swept semiconductor laser with a polygon-scanner-based wavelength filter," Optics Letters **28**, 1981-1983 (2003).
24. W.Y. Oh, S.H. Yun, G.J. Tearney, and B.E. Bouma, "115 kHz tuning repetition rate ultrahigh-speed wavelength-swept semiconductor laser," Opt. Lett. **30**, 3159-3161 (2005).
25. W.Y. Oh, S.H. Yun, B.J. Vakoc, G.J. Tearney, and B.E. Bouma, "Ultrahigh-speed optical frequency domain imaging and application to laser ablation monitoring," Appl. Phys. Lett. **88**, 103902-103904 (2006).
26. B.J. Vakoc, G.J. Tearney, and B.E. Bouma, "Real-time microscopic visualization of tissue response to laser thermal therapy," J. Biomed. Opt. **12**, 020501-020503 (2007).
27. I.K. Jang, B.E. Bouma, D.H. Kang, S.J. Park, S.W. Park, K.B. Seung, K.B. Choi, M. Shishkov, K. Schlendorf, E. Pomerantsev, S.L. Houser, H.T. Aretz, and G.J. Tearney, "Visualization of coronary atherosclerotic plaques in patients using optical coherence tomography: comparison with intravascular ultrasound," J. Am. Coll. Cardiol. **39**, 604-609 (2002).
28. I.K. Jang, G.J. Tearney, B. MacNeill, M. Takano, F. Moselewski, N. Iftimia, M. Shishkov, S. Houser, H.T. Aretz, E.F. Halpern, and B.E. Bouma, "In vivo characterization of coronary atherosclerotic plaque by use of optical coherence tomography," Circulation **111**, 1551-1555 (2005).
29. H. Yabushita, B.E. Bouma, S.L. Houser, H.T. Aretz, I.K. Jang, K.H. Schlendorf, C.R. Kauffman, M. Shishkov, D.H. Kang, E.F. Halpern, G.J. Tearney, "Characterization of human atherosclerosis by optical coherence tomography," Circulation **106**, 1640-1645 (2002).
30. G.J. Tearney, I.K. Jang, and B.E. Bouma, "Optical coherence tomography for imaging the vulnerable plaque," J. Biomed. Opt. **11(2)**, 021002 (2006).
31. R. Virmani, F.D. Kolodgie, A.P. Burke, A. Farb, and S.M. Schwartz, "Lessons from sudden coronary death: a comprehensive morphological classification scheme for atherosclerotic lesions," Arterioscler. Thromb. Vasc. Biol. **2000;20**, 1262-1275 (2000).

#86630 - $15.00 USD Received 20 Aug 2007; revised 7 Nov 2007; accepted 21 Nov 2007; published 14 Jan 2008

1. Introduction

Polarization sensitive optical coherence tomography (PS-OCT) [1-4] allows the determination of birefringence magnitude and orientation and polarization-dependent scattering and attenuation coefficients [2-4], information that is complementary to reflectance-based images provided by standard OCT. This capability has proven particularly powerful in biomedical applications, enabling the diagnosis of pathology and injury in cases where morphology alone is insufficient. Examples include the determination of burn depth in skin [5, 6], early diagnosis of glaucoma through quantification of retinal birefringence [7-9], identification of skin tumor [10] and the detection of dental caries lesions [11]. A recent preclinical study [12] demonstrated *ex vivo* that PS-OCT can be used to determine collagen content and smooth muscle cell density in atherosclerotic plaques. These parameters are thought to play a central role in determining the structural integrity of coronary plaques and their measurement in living patients would advance the understanding of plaque rupture and could guide the development of new therapeutics designed to stabilize plaques against disruption.

Early PS-OCT systems utilized free-space optics in the interferometer and sample arms and were configured to illuminate the sample with circularly polarized light to ensure that the incident polarization state did not coincide with the presumed linear birefringence axis of the sample [1, 2]. In fiber-based systems, and especially when using endoscopic or catheter-based probes, it is impractical to maintain a pre-determined polarization state at the tissue surface as the probe bends or rotates. This hurdle has been overcome by modulating the polarization state of the light at the sample so that it alternates between two states, which are perpendicular to each other on the Poincare sphere, on successive axial scans (A-lines) [4, 11, 12]. Each pair of successive polarization measurements forms a single axial birefringence profile of the sample via either Stokes vector analysis [14] or Jones matrix analysis [15]. However, in endoscopic or catheter-based imaging, sample motion or stress-induced birefringence changes in the fiber-optic probe can be non-negligible during the time interval between successive A-lines [16].

By taking advantage of the improved sensitivity and faster A-line rates of spectral-domain OCT, polarization-sensitive imaging at an A-line rate of 18.5 kHz has been demonstrated in a fiber-based system (PS-SD-OCT) [17]. Optical frequency domain imaging (OFDI) [18] is an alternative implementation of Fourier OCT and is conceptually a 2- or 3-dimensional extension of optical frequency domain reflectometry (OFDR) [19]. Taking advantage of the high detection sensitivity of OFDI, catheter-based reflectance imaging *in vivo* has been recently demonstrated at A-line rates of 64 kHz and frame rates up to 108 images per second [20]. Polarization-sensitive imaging has been demonstrated with OFDI using the standard approach of alternating polarization states between consecutive A-lines with a 500 Hz A-line rate [21].

In this paper, we describe a method for high-speed polarization-sensitive OFDI and demonstrate its use with both a microscope-type scanner and through a rotational catheter that is suitable for intracoronary application. A novel frequency-multiplexing scheme, leveraging the unique features of OFDI, enables simultaneous illumination and detection of two perpendicular polarization states on the Poincare sphere. This feature is particularly relevant for catheter-based polarization sensitive imaging, which can be prone to artifacts arising from stress-induced changes of birefringence during catheter rotation or bending [16]. Using a rotational fiber-optic catheter, we demonstrate polarization-sensitive imaging of a human coronary artery *ex vivo* at 62 kHz A-line rate and a frame rate of 123 images per second. The large ranging depth of 6.2 mm of the system accommodates the varying distances between the fiber-optic probe and the vessel wall that are characteristic of catheter-based imaging.

#86630 - $15.00 USD Received 20 Aug 2007; revised 7 Nov 2007; accepted 21 Nov 2007; published 14 Jan 2008

2. Principle of PS-OFDI

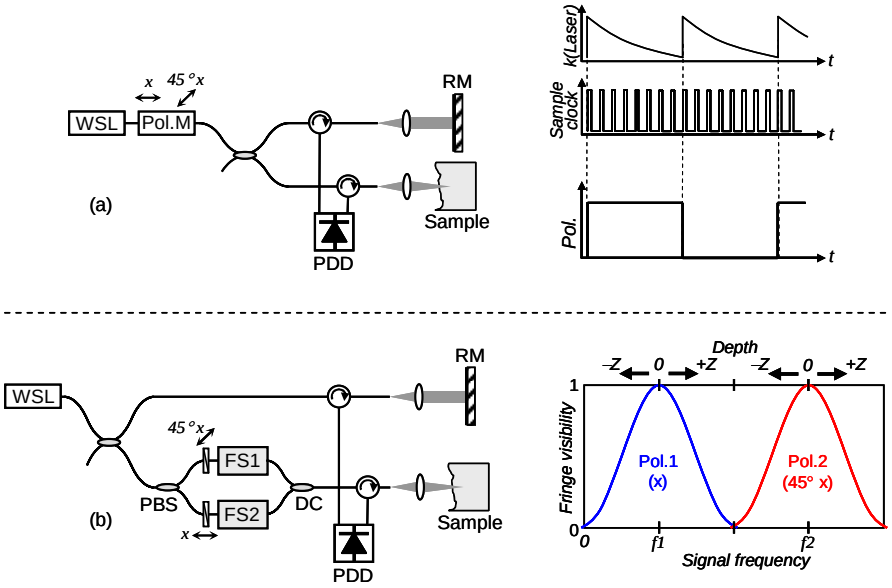

Fig. 1. Different schemes for PS-OFDI. (a) Conventional scheme, and (b) PS-OFDI with frequency multiplexing scheme. WSL, wavelength-swept laser; Pol.M, polarization modulator; RM, reference mirror; PDD, polarization diverse detection; PBS, polarization beam splitter; FS, frequency shifter; DC, directional coupler.

Figure 1(a) depicts the conventional PS-OFDI scheme, where the output of a wavelength-swept laser is modulated in a step-wise fashion between two perpendicular polarization states on the Poincare sphere in a pair of successive A-lines. Modulation is synchronous with the A-line acquisition rate. Polarization-diverse detection allows detecting all Stokes components of the light reflected from the sample.

An alternate scheme for PS-OFDI, which uses frequency multiplexing to simultaneously illuminate and detect a pair of perpendicular polarization states, is schematically represented in Fig. 1(b). In this approach, the light in the sample arm is split into two polarization states that are perpendicular to each other on the Poincare sphere. Each state is then encoded with a distinct frequency shift through the use of a frequency modulator prior to recombining the paths at a directional coupler. Since the two polarization states occupy different electrical frequency bands, the two polarization channels can be acquired simultaneously and demultiplexed in data processing, while additionally removing depth degeneracy [22]. The cross-sectional birefringence map is obtained from the Stokes vector components acquired from the two axial profiles via polarization diverse detection [14].

#86630 - $15.00 USD Received 20 Aug 2007; revised 7 Nov 2007; accepted 21 Nov 2007; published 14 Jan 2008

3. System configuration

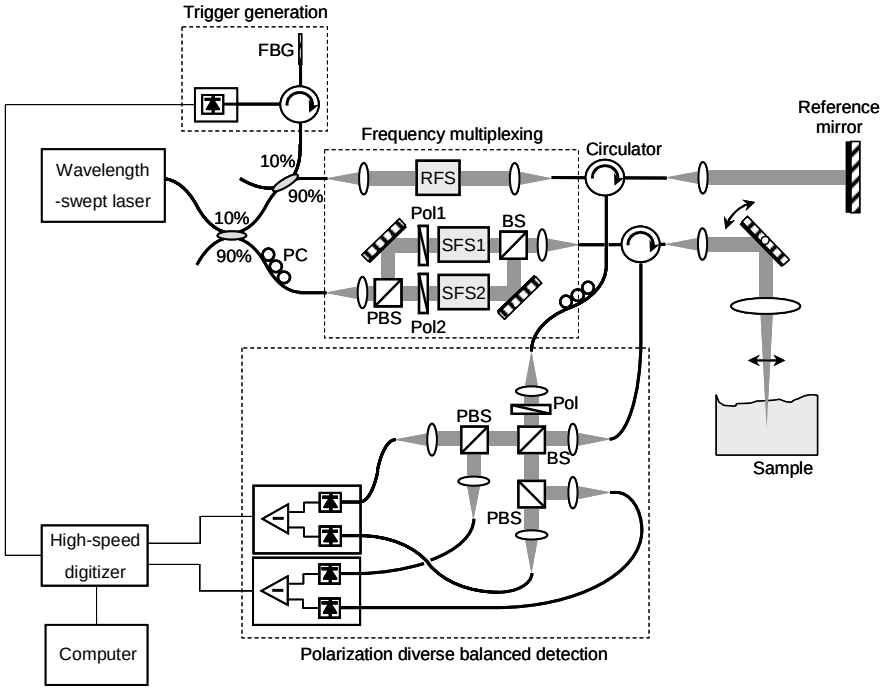

Fig. 2. Schematic diagram of PS-OFDI system. FBG, fiber Bragg grating; PC, polarization controller; RFS, reference arm frequency shifter; SFS1, sample arm frequency shifter; SFS2, AMTIR glass block for dispersion matching; PBS, polarization beam splitter; Pol, polarizer; BS, beam splitter.

Figure 2 depicts a PS-OFDI system that was constructed based on the frequency-multiplexing scheme. A wavelength-swept laser was constructed using a polygon scanning filter, providing polarized light with a wavelength sweep range of 1245 nm ~ 1355 nm. The laser was operated with a sweep repetition rate of 62 kHz and an instantaneous linewidth of 0.14 nm, which corresponds to an axial ranging depth of 5.2 mm (the range within 6 dB sensitivity from the zero delay depth) [23, 24]. The average power of the laser source was 54 mW. Ten percent of the laser output was directed to the reference arm of the system interferometer, and a small portion of the reference light was tapped to generate a trigger signal for each A-line through the use of a fiber Bragg grating (FBG). The remaining 90 % of the laser light was coupled to the sample arm where it was further divided into two orthogonal polarization states with a polarization beam splitter. A pair of Glan-Thompson polarizers in each light path reoriented these polarizations to be perpendicular in the Poincare sphere representation. Two frequency shifters (Brimrose Inc. AMF-25-1300 and AMF-50-1300) and an AMTIR glass block dimensionally matching those used in the frequency shifters were mounted in the system: a 25 MHz frequency shifter was placed in the reference arm and the glass block and 50 MHz frequency shifter were placed in the sample arm Mach-Zehnder interferometer. Driving frequencies of the frequency shifters were determined to ensure Nyquist sampling and minimum crosstalk between the two polarization states. Since the large size beam in the sample arm Mach-Zehnder interferometer reduces the cross-talk between adjacent diffraction orders but at the same time increases the wavelength dependent loss, the beam size was carefully selected through experimental measurement. With a high-speed and high-resolution digitizer (National Instruments PCI-5124, 200 MS/s, 12 bits), each polarization state was acquired over a 50 MHz frequency band centered at 25 MHz and 75 MHz, respectively. The experimental imaging range depends on the A-line rate and the sampling rate of the system, and the resulting image ranging depth of the system was 6.2 mm at 62 kHz A-line rate. For

#86630 - $15.00 USD Received 20 Aug 2007; revised 7 Nov 2007; accepted 21 Nov 2007; published 14 Jan 2008

stable and accurate phase measurement, the frequency shifter drivers were phase-locked with a clock signal from the digitizer. When imaging exposed specimens, a galvanometric mirror was used to provide transverse scanning over the sample. The average power on the sample was 9 mW and the $1/e^2$ spot size of the scanning beam was 32 μm. For intracoronary imaging, the scanner was replaced by an optical rotary junction and catheter as described below. A polarization-diverse detection scheme was implemented with balanced detectors (Thorlabs PDB110C, 100 MHz) for reduction of source RIN and auto-correlation noise [20]. A linear polarizer with a rotation angle of 45 degree was placed at the input port of the polarization diversity setup to ensure the same reference arm power for the detection of two orthogonal polarization states at each balanced receiver.

4. Polarization-sensitive imaging

4.1 Various tissue samples

Various biological samples were imaged as shown in Fig. 3. The axial resolution of the system was 9.8 μm in air, and the sensitivity was measured to be 107 dB at an A-line acquisition rate of 50 kHz. Each image frame contains 504 depth profiles spanning a width of 2 cm with a separation between adjacent A-lines of 1.24 times larger than the beam spot size and a depth of 7 mm. Figure 3(a) and (b) show intensity and phase retardation images of two different areas of chicken leg muscle tissue *ex vivo*. While the intensity images show relatively homogeneous structures in the sample, the phase retardation images show periodic banding structure in axial direction as the amount of phase retardation wraps several times between 0° and 180°, corresponding to the existence of strong birefringence in the tissue. In comparison, the image of the ventral surface of a human finger *in vivo* [Fig. 3(c)] indicates a more heterogeneous birefringence map with little polarization variation in the stratum corneum and axially and transversally varying birefringence in the epidermis and superficial dermis.

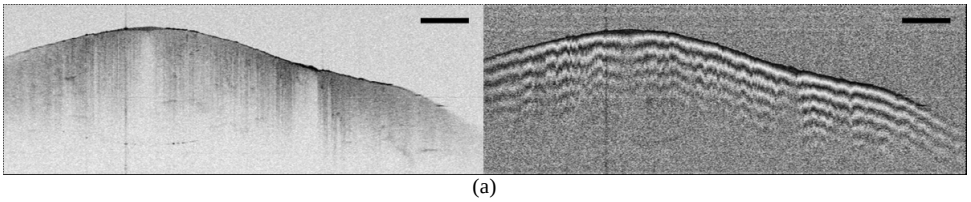

(a)

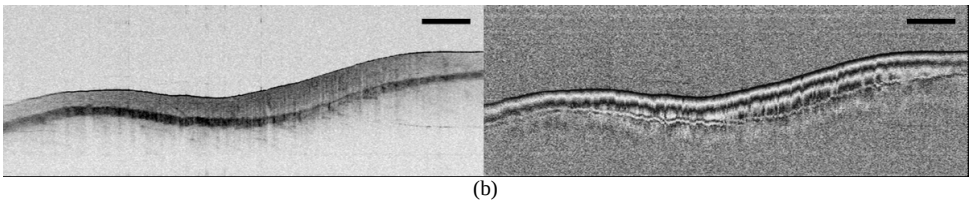

(b)

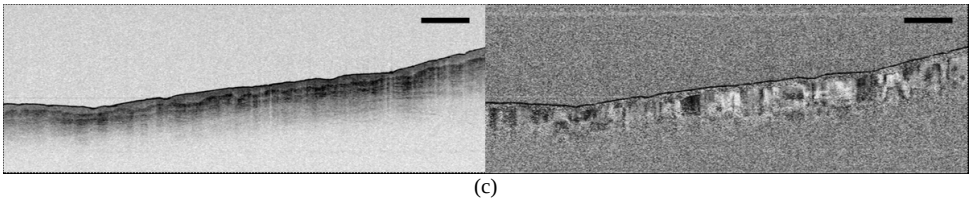

(c)

Fig. 3. Intensity and phase retardation images of (a) and (b) chicken muscle *ex vivo*, and (c) human finger *in vivo*. A-line rate: 50 kHz, imaging speed: 99 fps, image size: 2 cm (transverse) × 7 mm (axial), scale bar: 2mm.

#86630 - $15.00 USD Received 20 Aug 2007; revised 7 Nov 2007; accepted 21 Nov 2007; published 14 Jan 2008

4.2 Dynamic monitoring of tissue burn

The fast imaging speed of PS-OFDI offers the possibility of monitoring dynamic processes such as laser-induced coagulation of tissue [25, 26]. From prior studies, which investigated the use of PS-OCT to detect burn depth in skin [6], it is known that thermal denaturation of collagen and muscle can give rise to birefringence loss. To demonstrate the potential of PS-OFDI for monitoring such changes in real-time, we adapted the system of Fig. 2 to permit simultaneous laser irradiation and PS-OFDI. Figure 4 presents a sequence of 102 images of chicken muscle during exposure to cw laser heating (1.0 mm $1/e^2$ beam diameter at 1450 nm, 600 mW average power). All frames were acquired sequentially over a total duration of 0.73 seconds (138.9 fps). Each image comprises 360 A-lines covering a width of 2.8 mm. The loss of birefringence, starting at the surface and initially localized to the transverse extent of the 1450 nm laser beam, propagates with continued heating as would be expected to result from thermal denaturation of the tissue.

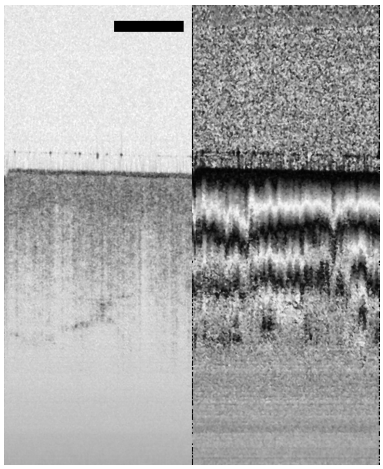

Fig. 4. Movie of a series of cross-sectional intensity and phase retardation images of chicken muscle tissue during laser ablation (below vaporization threshold). A-line rate: 50 kHz, imaging speed: 139 fps, presented at 20 fps, image size: 2.8 mm (transverse) × 7 mm (axial), scale bar: 1mm.

4.3 Intracoronary imaging ex vivo through rotational fiber-optic catheter

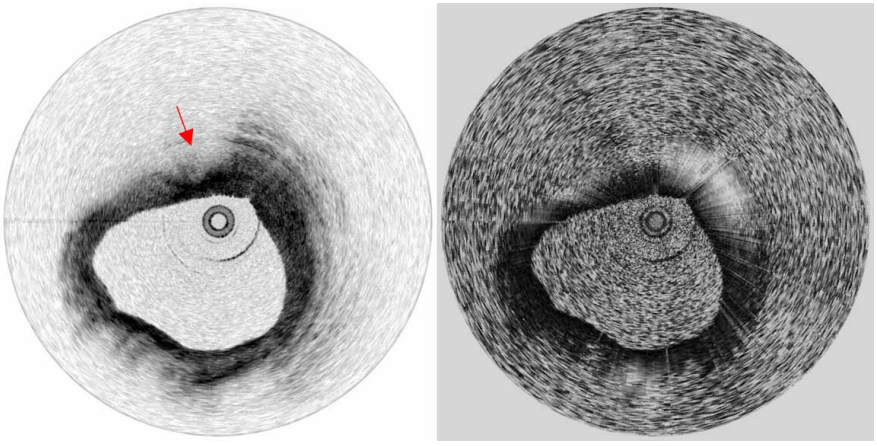

Fig. 5. Movie of a human coronary artery *ex vivo* acquired during a pull-back of 8 mm. Arrow: lipid-rich plaque. A-line rate: 62 kHz, imaging speed: 123 fps, presented at 6 fps.

#86630 - $15.00 USD Received 20 Aug 2007; revised 7 Nov 2007; accepted 21 Nov 2007; published 14 Jan 2008

To evaluate the potential of the frequency-multiplexed PS-OFDI system for catheter based imaging, an optical rotary junction and rotational catheter described previously [20] were used. Briefly, the rotary junction comprised a cylindrical housing with a pair of opposed collimating lenses; one collimator was held fixed and the second was free to rotate in a bearing. A motor was connected by a drive belt to the bearing, permitting rotational speeds of up to 8,000 rotations/min under computer control. The fiber pigtailed, rotational collimator was terminated with an optical connector matching that of the catheter. The imaging catheter comprised a non-rotating outer sheath and a drive shaft that enclosed an optical fiber. The distal end of the fiber included a pure silica segment for beam expansion, a facet polished at 41 degrees for total internal reflection, and an aspheric refractive face for focusing the beam to a ~30 μm spot transversely to the long axis of the catheter [20]. The proximal end of the catheter sheath included a telescoping section for helical pullback imaging.

Human coronary arteries were obtained post-mortem for imaging. After insertion of the catheter inside the vessel lumen, the outer sheath of the catheter was fixed with respect to the vessel and imaging was performed by rotating the drive shaft at a speed of 7,380 rotations/min, yielding a frame rate of 123 images/s. The driveshaft was also translated longitudinally within the sheath for three-dimensional pullback imaging. The PS-OFDI system was configured to acquire individual A-lines at a rate of 62 kHz and collected 504 A-lines per image (rotation) with the corresponding image ranging depth of 6.2 mm. A series of circular sections were acquired at a pitch of 100 μm in 0.65 s during a pull-back of 8 mm as shown in Fig. 5. Simultaneous acquisition of both intensity and birefringence data ensured absolute registration of these two image sets. The vessel structure and the plaque components were characterized using criteria that were previously determined and validated [27-30]. While the intensity images show distinct structures of coronary artery, including the layered structure of the vessel wall (intima, media, and adventitia, and internal and external elastic laminae) in relatively normal regions and fibrous and lipid-rich plaques [27-31], the birefringence (phase retardation) images help to differentiate lipid-rich plaques from thick fibrous plaques and calcific nodules. Midway through the movie of Fig. 5, for example, a lesion exhibiting features consistent with those of a lipid-rich plaque [29] is observed, spanning the sector from 10 o'clock past 12 o'clock. This sector exhibits low birefringence in comparison to the adjacent sector (12 o'clock through 2 o'clock), consistent with the distinction between lipid-rich and fibrous areas [12]. Although these observations are qualitative, it is important to note that periodic circumferential artifacts that could result from stress variations in the optical fiber during rotation are not observed in the images.

6. Conclusion

Cross-sectional birefringence images of biological tissue obtained by PS-OCT can provide information that is complementary to reflectance-based structural imaging alone. While recent studies have shown the potential of PS-OCT for evaluating the composition and mechanical integrity of coronary plaques *ex vivo*, high-speed intravascular birefringence imaging through a catheter has not previously been demonstrated. In this paper, we have presented a novel PS-OFDI scheme that uses frequency-multiplexing of two perpendicular polarization states on the Poincare sphere and that allows high-speed polarization sensitive imaging. With the help of simultaneous illumination and detection of two perpendicular polarization states in the high-speed PS-OFDI system, we have demonstrated polarization-sensitive imaging of a human coronary artery *ex vivo* at a frame rate of 123 images per second through a flexible fiber-optic catheter. We believe high-speed PS-OFDI may play an important role in future clinical studies investigating the role of plaque composition and structural integrity in acute myocardial infarction.

Acknowledgements

This research was supported in part by the US National Institutes of Health (contract R01 HL076398) and by the Terumo Corporation.

#86630 - $15.00 USD Received 20 Aug 2007; revised 7 Nov 2007; accepted 21 Nov 2007; published 14 Jan 2008